Cobalt and zinc halide complexes of 4-chloro and 4-methylaniline: syntheses, structures and magnetic behavior

Jonathan E. Chellali,[a] Cailyn Keely,[a] Graham Bell,[a] Kimberly L. Dimanno,[a] Tran Tran,[a] Christopher P. Landee,[b] Diane A. Dickie,[c]1 Melanie Rademeyer,[d] Mark M. Turnbull*[a] and Fan Xiao[e,f]*

[a] Carlson School of Chemistry and Biochemistry and

[b] Dept. of Physics, Clark University, 950 Main St., Worcester, Massachusetts 01610 USA

[c] Dept. of Chemistry, Brandeis University, 415 South St., Waltham, Massachusetts, 02453, USA

[d] Dept. of Chemistry, University of Pretoria, Private Bag X20, Hatfield 0028 South Africa

[e] Laboratory for Neutron Scattering and Imaging, Paul Scherrer Institut, CH-5232 Villigen PSI, Switzerland

[f] Department of Chemistry and Biochemistry, University of Bern, CH-3012 Bern, Switzerland

ABSTRACT: A family of cobalt(II) and zinc(II) compounds with the general formula (4-sub$C_6H_4NH_2)_2MX_2$, (M = Co, Zn; X = Cl, Br; sub = CH_3, Cl) has been prepared and the compounds characterized by single-crystal X-ray diffraction. The eight compounds crystallize in the monoclinic space group *I*2/a and are isocoordinate, but show different crystal packing for the 4-methyl and 4-chloroaniline complexes as a result of halogen bonding in the 4-chloroaniline family. The cobalt complexes have also been studied via variable temperature magnetic susceptibility measurements. All four Co(II) compounds exhibit antiferromagnetic exchange (maxima in χ are observed) and have been fitted with a 1D-chain model (cobalt chloride complexes, J ~ -3 K) or a 2D-model (cobalt bromide complexes, J ~ -4 K). Analysis of potential superexchange pathways is provided.

INTRODUCTION

The study of magnetism in the context of coordination chemistry has long been of interest and investigations aimed at understanding magnetostructural relationships, both experimental and theoretical, have received great attention over the past several years.[1,2,3] Extensive work has been done

1) Present address: Dept. of Chemistry, University of Virginia, 409 McCormick Road, Charlottesville, VA 22904 USA

recently, especially in the study of transition metal and lanthanide complexes, as a result of the discovery of single molecule, [4,5,6,7,8] single chain,[9,10,11] and single ion magnets.[12,13,14,15] Recent publications have demonstrated the breadth of interest in studies of molecular magnetic materials employing a wide variety of transition metal and lanthanoid ions.[16,17,18,19,20,21,22] One ongoing area of research in molecular magnetism has focused on transition metal halide complexes with a variety of N-donor ligands including substituted pyridines[23,24,25] and pyrimidines,[26,27] among others. We have been particularly interested in these types of complexes and their salts employing heterocyclic ligands such as substituted pyridines,[28,29,30] quinoline,[31,32] and isoquinoline.[33] Aromatic amines, such as aniline, also have significant potential for the preparation of complexes of this type. Aniline and substituted aniline compounds have been examined both for their qualities as Lewis bases[34] and in studies of how their basicity affects reactions and reaction mechanisms in the synthesis of complexes with the formula ML_2X_2 (X = Cl, Br; L = aniline-based ligand).[35] A wide variety of transition metal halide complexes of aniline itself have been reported including first-row transition metals such as Co,[36] Cu,[37] and Zn[38] as well as heavier transition metals such as Pd,[39] and Cd.[40] Work has also been reported on substituted aniline complexes, especially with substituents in the 4-position such as methyl,[41] ethyl,[42] and a number of halogens.[43] In spite of the significant body of work reported, there has been virtually no information published regarding the magnetic properties of these materials and the potential relationships between their structures and those magnetic properties. Thus we began a study to examine the magnetostructural relationships of such materials and here present our initial work with Co(II) and Zn(II) halide complexes of 4-chloro and 4-methylaniline. Although the Zn(II) compounds are diamagnetic it is frequently useful to have diamagantic analogues for comparison to the corresponding paramagnetic systems and thus they were included in this research.[44] Here we report the synthesis, characterization and single crystal X-ray structures of $(4\text{-sub}C_6H_4NH_2)_2MX_2$, (**1**, M = Co, X = Cl, sub = CH_3; **2**, M = Zn, X = Cl, sub = CH_3; **3**, M = Co, X = Br, sub = CH_3; **4**, M = Zn, X = Br, sub = CH_3; **5**, M = Co, X = Cl, sub = Cl; **6**, M = Zn, X = Cl, sub = Cl; **7**, M = Co, X = Br, sub = Cl; **8**, M = Zn, X = Br, sub = Cl).

EXPERIMENTAL

$CoBr_2 \cdot 6H_2O$ was obtained from Aldrich Chemical Company; $ZnBr_2$ and $ZnCl_2 \cdot 4H_2O$ were purchased from Alfa Aesar; 4-chloroaniline was purchased from Acros Organics; 4-methylaniline was purchased from Eastman Chemical; $CoCl_2 \cdot 6H_2O$ and solvents were purchased from Fisher Chemical; all were used without further purification. Ethanol refers to 95% ethanol unless otherwise stated. IR spectra were recorded via ATR on a Perkin-Elmer Spectrum 100 IR spectrophotometer. X-Ray powder diffraction data were collected on a Bruker AXS-D8 X-ray Powder Diffractometer. Elemental analyses were determined by Marine Science Institute, University of California, Santa Barbara CA 93106.

Dichloridobis(4-methylanilino)cobalt(II) (1)

A) 4-Methylaniline (0.107 g, 1.00 mmol) was dissolved in 15 mL of 1-propanol to give a pale yellow solution which was added dropwise to a stirred, blue solution of $CoCl_2 \cdot 6H_2O$ (0.119 g, 0.500 mmol) in 15 mL of 1-propanol. Slow evaporation at room temperature of the resulting blue solution produced blue needles which were collected by filtration, washed with a small amount of cold 1-propanol and allowed to air-dry. A second crop was harvested after two additional weeks. Total yield, 0.120 g (70%).

B) 4-Methylaniline (0.107 g, 1.00 mmol) and $CoCl_2 \cdot 6H_2O$ (0.120 g, 0.504 mmol) were added to a mortar. A single drop of methanol was added to the solids which were then ground until the sample was dry. After three drop cycles, the final product was a uniform blue powder, 0.130 g (75%). Products from the two methods were the same according to IR and combustion analysis. CHN for $C_{14}H_{18}N_2Cl_2Co$, found (calc.) C: 47.82(48.57), H: 5.84(5.83), N: 7.90(8.09). IR (ν) 3279w, 3236w, 3137w, 3032vw, 2925vw, 1580br-w, 1512m, 1070s, 824m, 809s, 733w, 703w, 661m, 635m cm^{-1}.

Dichloridobis(4-methylanilino)zinc(II) (2)

4-Methylaniline (0.353 g, 3.42 mmol) was dissolved in 2 mL of hot ethanol. Solid $ZnCl_2 \cdot 4H_2O$ (0.367 g, 1.76 mmol) was added to the stirring solution in a single portion, generating a cream colored slurry. Additional ethanol was added with continued heating, near the boiling point, until the precipitate just dissolved. The solution was then allowed to cool, resulting in the formation of colorless crystals which were isolated by filtration, washed with cold ethanol and allowed to air-dry to yield 0.491 g (76%). Single crystals for X-ray purposes were grown by slow evaporation of a solution of **2** in 1-propanol. CHN for $C_{14}H_{18}N_2Cl_2Zn$, found (calc.) C: 48.25(47.96), H: 5.24(5.17), N: 8.03(7.99). IR (ν) 3269w, 3230w, 3136w, 3032vw, 2925vw, 1582m, 1512s, 1060s-br, 824m, 810s, 736w, 703w, 670m, 637m cm^{-1}.

Dibromidobis(4-methylanilino)cobalt(II) (3)

A solution of 4-methylaniline (0.447 g, 2.08 mmol) in 5 mL of EtOAc was added to a solution of $CoBr_2 \cdot 6H_2O$ (0.452 g, 1.38 mmol) in 5 mL of ethanol to yield a dark blue-purple solution. Crystals began to form almost immediately. The solution was cooled in an ice bath. The resulting crystals were isolated by filtration, washed with cold EtOAc and allowed to air-dry to give blue crystals, 0.370 g (61%). Crystals suitable for X-ray diffraction were grown from a mixture of ethanol/toluene (~1:5). CHN for $C_{14}H_{18}N_2CoBr_2$, found (calc.) C: 38.56(38.83), H: 4.10(4.19), N: 6.35(6.47). IR (ν) 3276w, 3228w, 3134w, 3033vw, 2923vw, 1575m, 1511s, 1067s-br, 823m, 808s, 735w, 704w, 656m, 633m cm^{-1}.

Dibromidobis(4-methylanilino)zinc(II) (4)

A solution of 4-methylaniline (0.858 g, 8.02 mmol) dissolved in 15 mL of acetone was added, with stirring, to a solution of $ZnBr_2$ (0.771 g, 3.43 mmol) in 15 mL of acetone resulting in a pale-yellow solution. The solution was allowed to evaporate slowly at room temperature. Colorless crystals were seen after 1 day. After 1 week, the mixture was filtered and the crystals washed with n-hexane and allowed to air-dry to yield 1.275 g (84%). CHN for $C_{14}H_{18}N_2ZnBr_2$, found (calc.) C: 38.28(38.26), H: 4.04(4.13), N: 6.34(6.37). IR:ν 3284w, 3233m, 3131w, 3031w, 2922w, 1575m, 1512s, 1211w, 1065s-br, 823m, 808s, 735w, 704w, 660m, 634m cm^{-1}.

Dichloridobis(4-chloroanilino)cobalt(II) (5)

A solution of 4-chloroaniline (1.22 g, 9.6 mmol) dissolved in 12 mL of 1:1 ethanol:petroleum ether was added to a solution of $CoCl_2 \cdot 6H_2O$ (0.655 g, 2.70 mmol) dissolved in 6 mL of ethanol causing the rapid formation of a fine purple precipitate. Upon vacuum filtration, the purple precipitate began to quickly turn to dark blue; the transformation was complete within ~ 1 minute. The precipitate was washed with petroleum ether and the dark blue solid allowed to air-dry to yield 1.343 g (70 %). Crystals suitable for X-ray diffraction were grown by slow evaporation from ethanol. CHN for $C_{12}H_{12}N_2Cl_4Co$, found (calc.) C: 36.82(37.43), H: 2.95(3.14), N: 6.91(7.27). IR:ν 3280m, 3235m, 3137w, 1588m, 1492s, 1426w, 1215w, 1094m, 1066s, 1014m, 821s, 700w, 661m, 643m, 628m cm^{-1}.

Dichloridobis(4-chloroanilino)zinc(II) (6)

A solution of 4-chloroaniline (1.49 g, 11.7 mmol) in 5 mL of ethanol was added dropwise to a solution of anhydrous $ZnCl_2$ (0.53 g, 3.89 mmol) in 10 mL of ethanol with stirring. A precipitate began to form quickly. After one hour, the mixture was filtered, the precipitate washed with cold ethanol and it was allowed to air-dry to yield a white solid, 1.18g (77%). Crystals suitable for X-ray diffraction were grown by slow evaporation from ethanol. CHN for $C_{12}H_{12}N_2Cl_4Zn$, found (calc.) C: 36.75(36.81), H: 3.08(3.09), N: 7.13(7.13). IR:ν 3285m, 3240m, 3139w, 1580m, 1492s, 1425w, 1214w, 1095m, 1066s, 1014m, 821s, 701w, 666m, 643m, 628m cm^{-1}.

Dibromidobis(4-chloroanilino)cobalt(II) (7)

A warm solution of 4-chloraniline (0.260 g, 2.04 mmol, 5.0 mL) in tert-butyl alcohol (~50°C) was prepared and added to a mixture of $CoBr_2$ (0.238 g, 1.09 mmol) in 9.5 mL of warm tert-butyl alcohol (~50°). The temperature was raised to 70℃ and the solution was stirred until all of the $CoBr_2$ dissolved. The solution was allowed to cool and after 1 day dark blue crystals had formed. After 2 days the mixture was vacuum filtered, and the recovered crystals washed with n-hexane and allowed to air-dry to yield 0.155 g (32%). CHN for $C_{12}H_{12}N_2Cl_2CoBr_2$, found (calc.) C: 29.81(30.41), H: 2.80(2.55), N: 5.62(5.91). IR:ν 3277w, 3228m, 3126w, 1574m, 1492s, 1094m, 1070s, 821s, 644mcm^{-1}.

Dibromidobis(4-chloroanilino)zinc(II) (8)

A) The synthesis was adapted from a previously reported procedure.[45] A solution of 4-chloroaniline (0.127 g, 0.992 mmol) in 15 mL of acetone was added dropwise to a solution of $ZnBr_2$ (0.115 g, 0.502 mmol) dissolved in 15 mL of acetone. The resulting colorless solution produced acicular clusters of white crystals after two weeks of slow evaporation at room temperature, 0.201 g (83%).

B) 4-Chloroaniline (0.128 g, 1.00 mmol) and $ZnBr_2$ (0.112 g, 0.498 mmol) were added to a mortar. A single drop of ethanol was added to the solids which were then ground until the sample was dry. After eight drop cycles, the final product was a uniform white powder, 0.205 g (85%). Products from the two methods were the same according to IR and combustion analysis. CHN for $C_{12}H_{12}N_2Cl_2ZnBr_2$, found (calc.) C: 29.34(30.00), H: 2.75(2.52), N: 5.55(5.83). IR (ν) 3278w, 3236w, 1580w 1512m, 1070s, 824m, 819s, 733w, 703w, 661m, 635m cm^{-1}.

2.2. Magnetic data

Magnetic data for compounds **1**, **3**, **5** and **7** were measured on a Quantum Design MPMS-XL magnetometer (SQUID). Crystals were powdered prior to measurements and powder X-ray diffraction used to confirm the phase of the material (by comparison with single crystal data) and purity (no unindexed peaks were detected). Samples were placed in a gelatin capsule which was then affixed inside a plastic straw. Magnetization was measured in applied fields ranging from 0 to 50 kOe. As the field was reduced back to zero, several data points were recollected to check for hysteresis; none was observed. M(H) was linear to at least 10 kOe for all samples measured. Magnetization was then measured between 1.8 and 310 K in an applied field of 1 kOe. All data were corrected for the background of the gelatin capsule and straw (measured independently) as well as the diamagnetic contributions of the constituent atoms, estimated via Pascal's constants.[46]

2.3. Single-crystal X-ray diffraction data

X-ray diffraction data for structures **1** – **4, 7** and **8** were collected on a Bruker D8 Venture Diffractometer equipped with a Photon 100 CMOS detector employing graphite-monochromated Mo-Kα radiation, using φ and ω scans. Data collections for **5** and **6** were carried out on a Bruker Kappa diffractometer fitted with an APEXII detector employing graphite-monochromated Mo-Kα radiation, using phi and omega scans. Data collection, reduction and absorption corrections were made using Bruker Instrument Services v.2012.12.0.3, SAINT v.8.34A and SADABS v.2014/5.[47] The structures were solved using SHELXS-97[48] and refined via least squares analysis with SHELXL-2014.[49] Non-hydrogen atoms were refined using anisotropic thermal parameters. Hydrogen atoms bonded to carbon were placed in calculated positions and refined using a riding model and isotropic thermal parameters. Hydrogen atoms bonded to nitrogen were located in the difference Fourier maps and their positions

refined with fixed isotropic thermal parameters. Crystallographic information for compounds **1-8** is given in Table 1. Selected bond lengths and angles are presented in Table 2 while hydrogen bonding parameters are shown in Table 3. The data have been deposited with the CCDC as 1854458(**5**), 1854459(**1**), 1854460(**2**), 1854461(**7**), 1854462(**6**), 1854463(**4**), 1854464(**3**), 1854465(**8**).

Table 1: Crystal and experimental data for **1-8**.

	1	**2**	**3**	**4**	**5**	**6**	**7**	**8**
Formula	$C_{14}H_{18}N_2Cl_2Co$	$C_{14}H_{18}N_2Cl_2Zn$	$C_{14}H_{18}N_2CoBr_2$	$C_{14}H_{18}N_2ZnBr_2$	$C_{12}H_{12}N_2Cl_4Co$	$C_{12}H_{12}N_2Cl_4Zn$	$C_{12}H_{12}N_2Cl_2CoBr_2$	$C_{12}H_{12}N_2Cl_2ZnBr_2$
MW (g/mol)	344.13	350.57	433.05	439.49	384.97	391.41	473.89	480.33
T(K)	150(2)	150(2)	150(2)	150(2)	120(2)	120(2)	150(2)	150(2)
λ (Å)	0.71073	0.71073	0.71073	0.71073	0.71073	0.71073	0.71073	0.71073
Crystal system	monoclinic	monoclinic	monoclinic	monoclinic	monoclinic	monoclinic	monoclinic	monoclinic
Space group	I2/a	I2/a	I2/a	I2/a	I2/a	I2/a	I2/a	I2/a
a (Å)	12.2722(7)	12.2525(15)	12.991(3)	12.9781(9)	12.2093(6)	12.2047(6)	13.0618(7)	13.0483(18)
b (Å)	4.6313(2)	4.6322(6)	4. 6666(8)	4.6676(3)	4.5559(2)	4.5516(2)	4.5747(3)	4.5796(6)
c (Å)	25.9938(14)	26.128(4)	25.770(5)	25.8403(17)	25.9368(14)	26.0210(15)	25.6954(14)	25.746(4)
β(˚)	92.995(3)	93.015(8)	92.013(10)	92.014(3)	93.452(3)	93.512(2)	92.585(3)	92.579(7)
V ($Å^3$)	1475.37(13)	1480.9(3)	1561.3(5)	1564.35(18)	1440.10(12)	1442.77(13)	1533.83(15)	1536.9(4)
Z	4	4	4	4	4	4	4	4
Size(mm)	0.060x0.105x0.270	0.25x0.12x0.05	0.48x0.06x0.04	0.176x0.222x0.374	0.62x0.08x0.07	0.32x0.09x0.09	0.066x0.128x0.166	0.082x0.235x0.357
Abs. co. (mm^{-1})	1.512	2.006	6.205	6.666	1.918	2.428	6.663	7.131
F(0,0,0)	708	720	852	864	772	784	916	928
Θ_{range} (˚)	3.139 to 26.521	3.123 to 27.414	3.138 to 27.162	3.141 to 26.491	1.573 to 30.508	1.568 to 28.291	3.122 to 26.508	3.126 to 26.517
Index ranges	-15≤ h≤ 15 -5≤ k≤ 5 -32≤ l≤ 32	-15≤ h≤ 15 -5≤ k≤ 5 -33≤ l≤ 32	-16≤ h≤ 16 -5≤ k≤ 5 -33≤ l≤ 33	-16≤ h≤ 16 -5≤ k≤ 5 -32≤ l≤ 32	-15≤ h ≤17 -6≤ k ≤5 -37≤ l ≤37	-16≤ h ≤16 -6≤ k ≤6 -34≤ l ≤34	-16≤ h≤ 16 -5≤ k≤ 5 -32≤ l≤ 32	-16≤ h≤ 16 -5≤ k≤ 5 -32≤ l≤ 32
Rfln. Coll.	19805	14664	26252	18341	9044	15547	18417	17991
Ind. rfln (R_{int})	1528 (0.0354)	1637 (0.0744)	1723 (0.0385)	1614 (0.0555)	2209 (0.0242)	1785 (0.0297)	1593 (0.0410)	1588 (0.0577)
Data/Res/ para	1528/0/94	1637/0/94	1723/0/94	1614/0/94	2209/0/93	1785/0/93	1593/0/93	1588/0/93
Final R (R1)	0.0203	0.0558	0.0207	0.0190	0.0226	0.0181	0.0165	0.0214
[I>2σ(I)] (wR2)	0.0504	0.1146	0.0527	0.0465	0.0569	0.0473	0.0377	0.0541
R index (R1)	0.0254	0.0726	0.0251	0.0227	0.0267	0.0205	0.0216	0.0275
(all data) (wR2)	0.0521	0.1208	0.0550	0.0481	0.0586	0.0473	0.0390	0.0558
Final peak/hole	0.245/	1.81(near	0.737/	0.467/	0.565/	0.357/	0.294/	0.732/
(e/$Å^3$)	-0.257	Zn1)/-0.95	-0.443	-0.452	-0.282	-0.242	-0.381	-0.464

Table 2: Bond Lengths (Å) and angles (˚) for **1-8**

Bond Lengths	**1**	**2**	**3**	**4**	**5**	**6**	**7**	**8**
M1-X1	2.2484(4)	2.2437(12)	2.3899(5)	2.3806(3)	2.2474(3)	2.2448(4)	2.3897(3)	2.3805(4)
M1-N11	2.0602(14)	2.059(4)	2.062(2)	2.0667(18)	2.0578(12)	2.0571(12)	2.0613(16)	2.071(2)
N11-C11	1.444(2)	1.448(6)	1.445(3)	1.443(3)	1.4424(17)	1.4437(18)	1.443(2)	1.440(3)

N11-H11A	0.85(2)	0.93(6)	0.84(3)	0.86(3)	0.844(19)	0.852(19)	0.86(2)	0.89(3)
N11-H11B	0.84(2)	0.83(6)	0.87(3)	0.83(3)	0.872(18)	0.850(19)	0.85(2)	0.74(3)
Bond Angles								
X1-M1-X1a	109.64(2)	109.67(6)	110.56(2)	111.282(16)	109.824(19)	109.699(19)	111.194(17)	111.926(19)
N11-M1-N11a	116.76(8)	117.3(2)	119.92(12)	119.81(10)	118.24(7)	119.04(7)	121.89(9)	121.46(11)
N11-M1-X1	107.46(4)	107.55(13)	106.04(7)	105.98(6)	107.40(4)	107.28(4)	106.36(5)	106.21(6)
N11-M1-X1a	107.70(4)	107.30(13)	107.09(6)	106.90(5)	106.91(3)	106.68(4)	105.49(5)	105.56(6)
M1-N11-C11	109.76(9)	110.2(3)	111.06(14)	111.58(12)	110.38(8)	111.10(9)	112.16(11)	112.21(14)

Symm. Op. a) 1-x, y, 0.5-z;

Table 3: Hydrogen bonding for compounds **1-8**

Compound	D-H···A	d(D-H)Å	d(H···A)Å	d(D···A)Å	<(DHA)°
1	N11-H11A···X1a	0.85(2)	2.69(2)	3.4003(15)	141.2(15)
	N11-H11B···X1b	0.84(2)	2.82(2)	3.3949(14)	127.7(15)
2	N11-H11A···X1a	0.93(6)	2.60(6)	3.404(4)	145(4)
	N11-H11B···X1b	0.83(6)	2.83(6)	3.410(4)	128(5)
3	N11-H11A···X1a	0.84(3)	2.82(3)	3.507(2)	141(2)
	N11-H11B···X1b	0.87(3)	2.88(3)	3.482(2)	127(2)
4	N11-H11A···X1a	0.86(3)	2.87(3)	3.4955(18)	131.0(19)
	N11-H11B···X1b	0.83(3)	2.83(3)	3.5170(19)	142(2)
5	N11-H11A···X1a	0.844(19)	2.664(18)	3.3672(12)	141.6(14)
	N11-H11B···X1b	0.872(18)	2.801(18)	3.3785(12)	125.1(13)
6	N11-H11A···X1a	0.852(19)	2.664(19)	3.3728(13)	141.5(15)
	N11-H11B···X1b	0.850(19)	2.810(19)	3.3863(13)	126.6(14)
7	N11-H11A···X1a	0.86(2)	2.85(2)	3.4653(16)	130.2(17)
	N11-H11B···X1b	0.85(2)	2.77(2)	3.4855(17)	141.8(18)
8	N11-H11A···X1a	0.89(3)	2.83(3)	3.478(2)	131(2)
	N11-H11B···X1b	0.74(3)	2.87(3)	3.494(2)	144(3)

Symm. Op.: a, x, y+1, z; b, -x+1/2,y+1,-z.

Table 4: Metal-halide short contacts in **1-8**

	1	**2**	**3**	**4**	**5**	**6**	**7**	**8**
X1···M1A (Å)	3.809	3.811	3.845	3.862	3.7465	3.741	3.780	3.799
M1-X1···M1A (°)	96.3	96.4	94.0	93.8	95.7	95.8	92.96	92.76

Table 5: Comparison of two-halide superexchange pathway parameters of **1-8**

	1	**2**	**3**	**4**	**5**	**6**	**7**	**8**
d (Å)	3.597	3.607	3.732	3.735	3.582	3.597	3.751	3.753
Θ (˚)	127.9	127.6	127.9	127.5	127.5	127.2	127.6	127.3

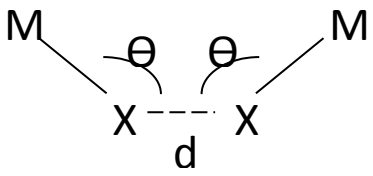

RESULTS

Syntheses

Reaction of 4-methylaniline or 4-chloroaniline with the appropriate metal halide (M = Co, Zn; X = Cl, Br) yielded the complexes **1-8** in yields ranging from 32-85% (Scheme 1). The reaction appears to be very tolerant of the reaction conditions; solution syntheses employing a variety of solvents and solvent mixtures (ethanol, ^{t}butyl alcohol, acetone, ethyl acetate) were effective, as well as mechanochemical[50] techniques. In some cases, slightly elevated temperatures were useful for solution syntheses, but primarily for improving the solubility of the starting metal halide in some solvents rather than affecting the reaction itself.

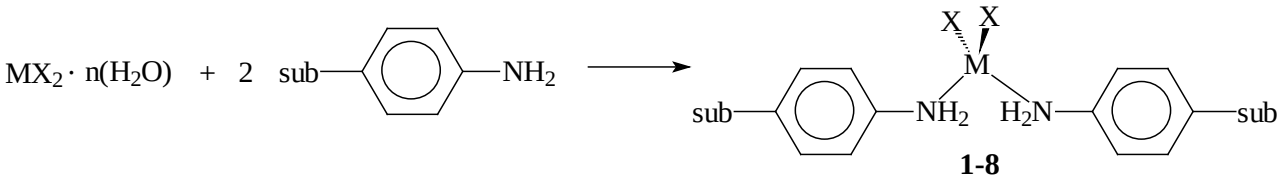

Scheme 1: The synthesis of compounds **1-8**, (4-sub$C_6H_4NH_2)_2MX_2$. (**1**, M = Co, X = Cl, sub = CH_3; **2**, M = Zn, X = Cl, sub = CH_3; **3**, M = Co, X = Br, sub = CH_3; **4**, M = Zn, X = Br, sub = CH_3; **5**, M = Co, X = Cl, sub = Cl; **6**, M = Zn, X = Cl, sub = Cl; **7**, M = Co, X = Br, sub = Cl; **8**, M = Zn, X = Br, sub = Cl).

In all cases, crystals suitable for single-crystal X-ray diffraction could be grown by slow evaporation of a solution (usually in an alcohol) of the compound at room temperature over several days (see Experimental for details).

Crystal Structures

All eight compounds crystallized in the monoclinic crystal system and were analyzed in the space group *I*2/a. The compounds are isostructural for a given ligand and thus details will be presented for one compound each of 4-methylaniline and 4-chloroaniline. Full details for all compounds are reported in the Tables and Supplementary Material.

Dichloridobis(4-methylanilino)cobalt(II) (1)

Compound **1** crystallized in the monoclinic space group *I*2/*a* with four molecules per unit cell. The asymmetric unit comprises one 4-methylaniline molecule, one chloride ion and ½ Co(II) ion which is located on a crystallographic two-fold axis. The molecular unit is shown in Figure 1. The Co(II) ion exhibits a slightly distorted tetrahedral geometry with a mean trans angle[51] of 113.1° (109.5° for tetrahedral, 180° for square planar) with the N11-Co1-N11A angle slightly larger than the Cl1-Co1-Cl1A angle. The pyridine ring is virtually planar (mean deviation of constituent atoms = 0.0044Å) with the carbon atom of the methyl substituent nearly in the same plane (0.0007Å) and N11 atom only slightly removed (0.0621 Å).

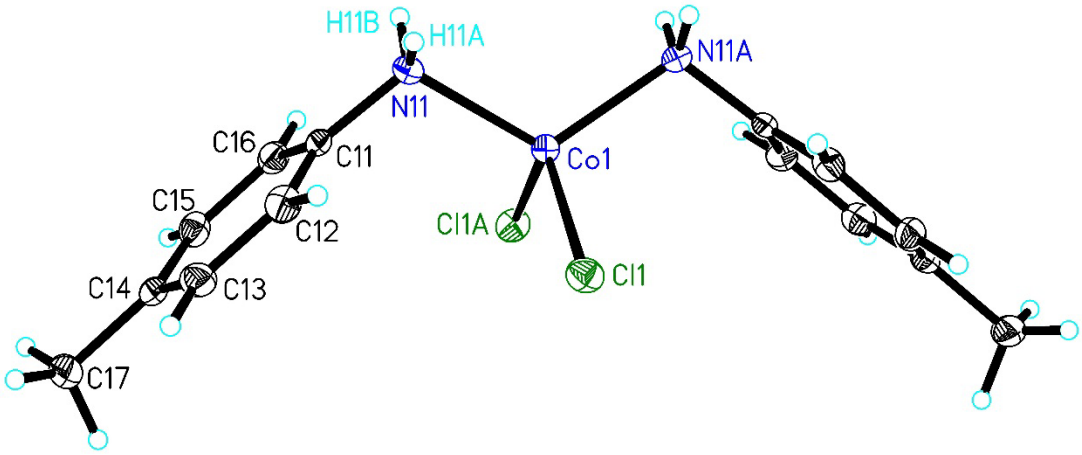

Figure 1: A plot of the molecular unit of compound **1** showing 50% probability thermal ellipsoids. Hydrogen atoms are shown as spheres of arbitrary size. The asymmetric unit, copper coordination sphere and only those hydrogen atoms whose positions were refined are labeled.

The molecular units are linked into chains parallel to the *b*-axis by a combination of hydrogen bonds and short, intermolecular Co···Cl contacts (Figure 2a, Tables 3 and 4). The amino group of each aniline ligand forms two nearly-symmetrical hydrogen bonds to the two chloride ions in the adjacent molecular unit ($d_{(D\cdots A)}$ = 3.394(1), 3.400(1) Å). The same pairs of molecular units also exhibit short Cl···Co intermolecular contacts which reinforce the hydrogen bonding ($d_{Cl1\cdots Co1b}$ = 3.809(2)Å, Figure 2a). The chains are further linked into layers via short Cl···Cl contacts (3.597(2)Å) roughly parallel to the *c*-axis

(Figure 2b). This results in alternating hydrophilic (Co, Cl, NH_2) and hydrophobic (Ph, CH_3) layers parallel to the A-face of the crystal.

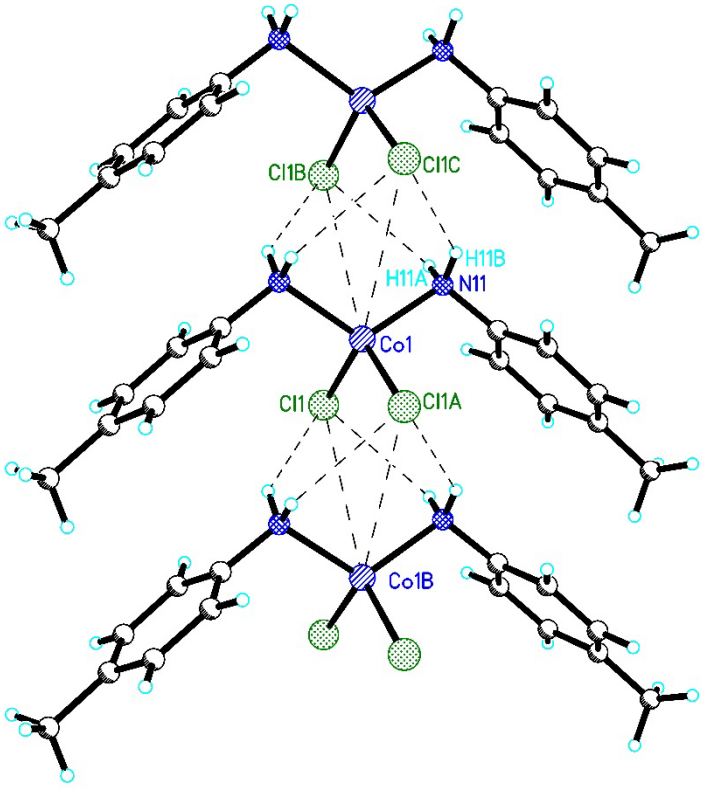

a)

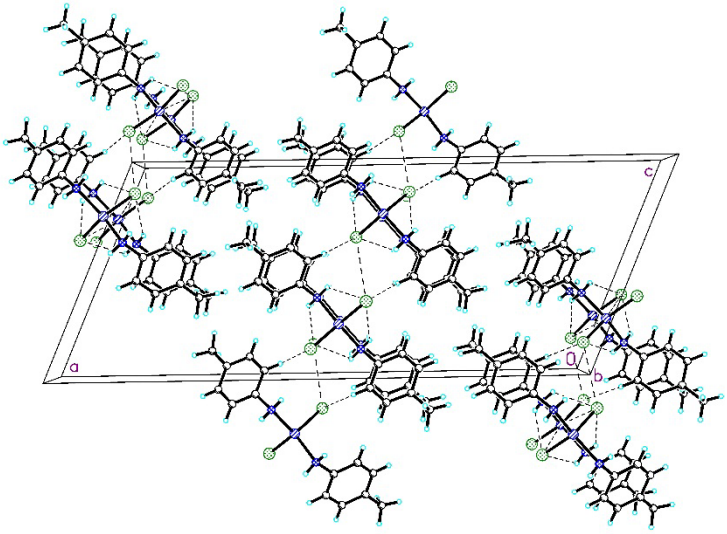

b)

Figure 2: a) The chain structure of **1** formed via hydrogen bonds and short Co···Cl contacts (both shown as dashed lines). b) The packing structure of **1** viewed parallel to the chains (*b*-axis). The dashed lines represent hydrogen bonds and short Cl···Cl contacts between chains.

Compounds **2-4** crystallize and pack in the same fashion. Figures showing the molecular units of **2-4**, Figures S1-S3 respectively, may be found in Supplementary Information.

Dichlorido-bis(4-chloroanilino)cobalt(II) (5)

Compound **5** crystallized in the monoclinic crystal class, as does **1**, and was solved and refined in the space group *I*2/a. The molecular unit (Figure 3) is isostructural with **1**. The Co-N and Co-Cl bond lengths are the same as those found in **1** within experimental error, but the N-Co-N and Cl-Co-Cl bond angles are slightly larger (by 1.5 and 0.2°, respectively) in **5**.

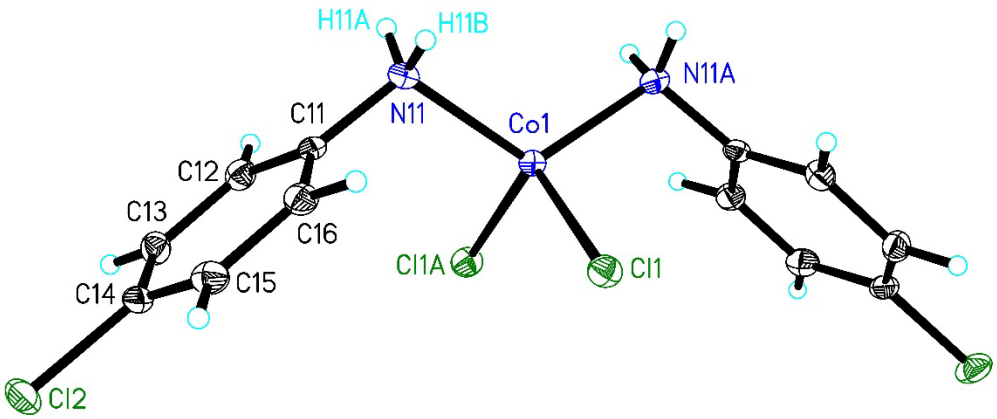

Figure 3: A plot of the molecular unit of compound **5** showing 50% probability thermal ellipsoids. Hydrogen atoms are shown as spheres of arbitrary size. The asymmetric unit, copper coordination sphere and only those hydrogen atoms whose positions were refined are labeled.

As with **1**, the molecules are stacked parallel to the *b*-axis and stabilized in that motif by a combination of hydrogen bonds (Table 3) and short Co···Cl contacts ($d_{Co\cdots Cl}$ = 3.746 Å; $\angle_{Co\cdots Cl\text{-}Co}$ = 95.7°). However, unlike in **1** there are halogen bonds between the adjacent stacks which modify the packing of the crystal (Figure 4). These are Type II halogen bonds with $d_{Cl2\cdots Cl2a}$ = 3.523 Å, $\angle_{C14\text{-}Cl2\cdots Cl2a}$ = 144.6° and $\angle_{Cl4\text{-}Cl2\cdots Cl2b}$ = 89.5° (Figure 4a).

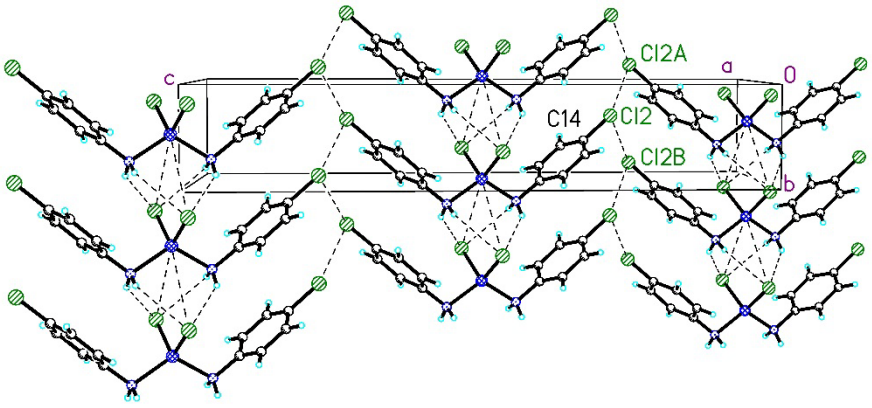

a)

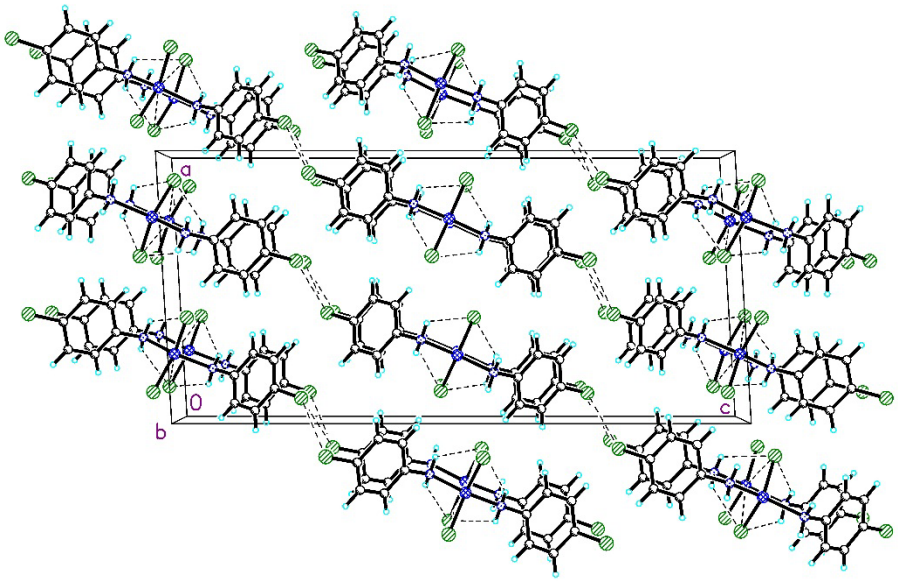

b)

Figure 4: Crystal packing of **5** viewed parallel to the a) *a*-axis and the b) *b*-axis. Dashed lines show hydrogen bonds, halogen bonds and short Co···Cl contacts.

Magnetic properties

The magnetic behavior of **1**, **3**, **5** and **7** can be qualitatively catagorized into two groups and each group is analyzed with a different approach. In **1** and **5**, two possible transitions are identified (T_1 can be extracted from the slope change in χ and T_2 can be located by examining χT) while in **3** and **7**, only one transition (T_1) can be seen and the curve closely resembles the conventional long range ordering of a low-dimensional magnetic system.

For **1** and **5**, three models were attempted to fit the magnetic data with two different temperature windows. Above the higher transition temperature (T_2), χ was fitted to the Curie-Weiss equation $\chi=C/(T+\theta_{CW})$, where C is the Curie constant and θ_{CW} is the Weiss temperature. The procedure yielded C_1=2.56(2) emu·K/mol, θ_{CW1}=-4.42(9) K, C_5=2.67(2) emu·K/mol and θ_{CW5}=-4.01(14) K (Note: C_1, θ_{CW1}, etc. represent results for compound **1**, C_5 … for compound **5**, etc.), indicating the presence of antiferromagnetic interactions in both compounds. Above the lower transition temperature (T_1), two isotropic antiferromagnetic models were applied: the one-dimensional S=3/2 antiferromagnetic chain (proposed by Fisher[52]) and the two-dimensional S=3/2 antiferromagnetic square lattice (empirical formula of χ constructed based on quantum Monte Carlo simulations,[53] detailed in SI-1 and Table SI1). The data and fits of **1** are plotted in Figure 5(a) and the equivalent plot of **5** is included in the Supplementary Information (Fig. SI7). In all three fits, the amount of paramagnetic impurity was fixed to zero (no paramagnetic tail is observed in the data). The extracted C, θ_{CW}, $J_{total}=zJ$ (z = number of nearest neighbors, J = exchange coupling strength in temperature units) are listed in Table 5.

For **3** and **7**, the more conventional χ was fitted to two models above the transition temperature T_1: the one-dimensional chain[52] and the two-dimensional antiferromagnetic rectangular lattice (with anisotropic interactions along two edges in the plane and the ratio between the two is defined as $\alpha=J'/J$, see Supplementary Information for more information). The data and fits of **3** are plotted in Figure 5(b) and the equivalent plot of **7** is in Figure SI8. Similarly, the amount of paramagnetic impurity was fixed to zero and the fitted parameters are listed in Table 5 for comparison.

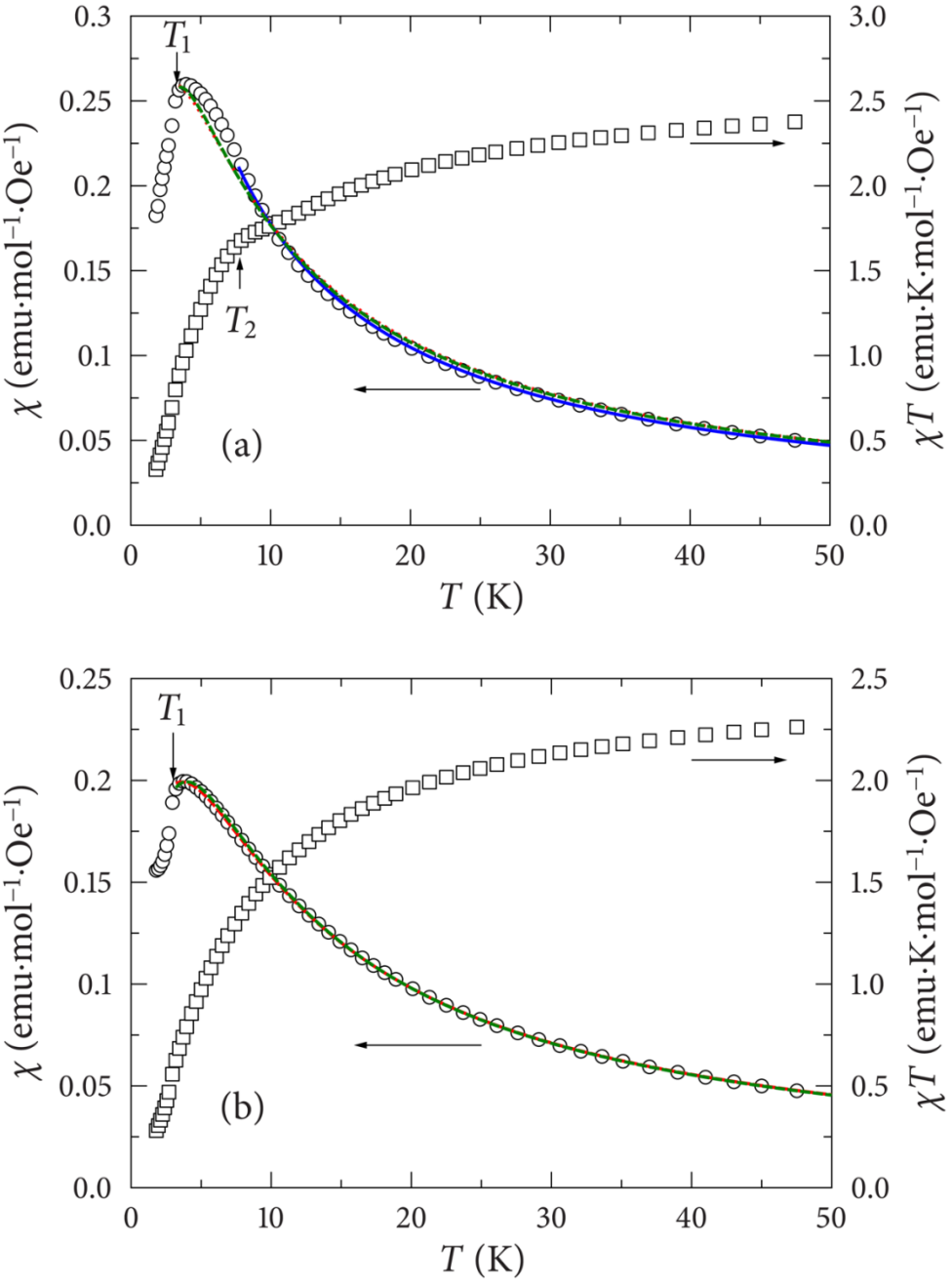

Figure 5: (a) Temperature dependence of χ (○) and χT (□) for **1** . The solid line, dotted line and dashed line are fits using the Curie-Weiss model, 1D chain model and 2D square lattice model, respectively. (b)

Temperature dependence of χ (○) and χT (□) for **3**. The dotted lines and dashed lines are fits using the 1D chain model and 2D rectangle lattice model, respectively.

Table 5: Fitting results for magnetic data of compounds **1**, **3**, **5** and **7**. The susceptibility of 1D Heisenberg chain model is from Ref. 52 and the 2D square lattice/rectangle models are formulated using simulations[53] (see SI for details). The sum of all *J*s (J_{total}) is used to compare with the Weiss temperature.

Compound	**Model**	**C (emu·K/mol)**	**θ_{CW} or J_{total} (K)**	**α**
1	Curie-Weiss	2.56(2)	-4.42(9)	
1	1D chain	2.66(1)	-3.28(2)	0
1	2D square lattice	2.67(1)	-3.57(2)	1
5	Curie-Weiss	2.67(2)	-4.01(14)	
5	1D chain	2.63(2)	-2.62(4)	0
5	2D square lattice	2.67(2)	-2.92(4)	1
3	1D chain	2.53(1)	-4.07(1)	0
3	2D rectangle	2.51(1)	-4.02(1)	0.15
7	1D chain	2.70(1)	-4.32(2)	0
7	2D rectangle	2.65(1)	-4.13(2)	0.10

DISCUSSION

Within experimental error, there are no differences in the bond lengths amongst the eight compounds with the obvious exception that the M-Br bonds are longer than the M-Cl bonds. Perhaps surprisingly, there are no differences between the M-N11 or N11-C11 bond lengths, indicating that there is no effect induced by the difference between the electron-donating methyl substituent and the electron-withdrawing chloro substituent. The X-M-X angles are slightly larger in the bromide complexes as are the N-M-N angles, most likely as a result of steric effects. The same is true of the M-N-C angle.

The structures of **1-8** are dominated by four distinct classes of intermolecular interactions. All of the compounds form chains parallel to the *b*-axis via hydrogen bonds and short halide···metal contacts. Considering the hydrogen bonding first, there are differences between the metal chloride compounds (**1,2,5,6**) and the metal bromide compounds (**3,4,7,8**) as expected. In the chloride complexes, the D···A distances (~3.4 Å) are ~0.1 Å shorter than those observed in the bromide complexes (~3.5 Å) as would be expected given the smaller radius of the chloride ion. More interesting, however, is the fact that there is a small difference in D···A distances observed for the 4-methylaniline compounds compared to the 4-chloroaniline compounds, but no difference is observed as a function of the metal ions. For

example, the D···A distances for **1** (Co, Cl; 3.3944(14), 3.4003(15) Å) and **2** (Zn, Cl; 3.404(4), 3.410(4) Å), both 4-methylaniline complexes, are the same within experimental error. However, the average D···A distance for **1** and **2** (3.402(3) Å) is slightly longer than the average D···A distance (3.3762(15) Å) in the equivalent 4-chloroaniline complexes **5** and **6**. The same trend is observed for the bromide complexes. The short metal···halide contacts between adjacent molecules along the *b*-axis mirror the differences seen in the hydrogen bonding. The M···X distances are slightly shorter (~0.04 Å) for the chloride complexes than for the bromide complexes, as expected, and are also slightly shorter for the 4-chloroaniline complexes than for the 4-methylaniline complexes (~0.04 Å) as was seen in the hydrogen bonding. Further, this is in agreement with the observation that the *b*-axis length for the 4-chloroaniline complexes is ~0.1 Å shorter than in the equivalent 4-methylaniline complex. This type of stacking interaction appears to be a common motif in this class of molecules when the geometry at the metal ions is tetrahedral and is observed in the corresponding complexes of aniline itself with $ZnBr_2$,[38a] ZnI_2,[38b] $CoCl_2$,[36] and CdI_2.[40a] However, when the ML_2X_2 complex is square planar, the phenyl rings orient themselves on opposite sides of the coordination plane and a different type of chain structure is formed where the halide ions exhibit short contacts to two different adjacent molecules. This alternate packing structure is observed in complexes of Pd,[39a,43a] and Cu.[37,54]

The third intermolecular interaction observed in the complexes is the two-halide superexchange pathway which links adjacent chains parallel to the *c*-axis. The four potential parameters for the two-halide pathway (d, θ_1, θ_2, T) are reduced to only two different parameters, d and θ (Table 5), because $\theta_1 = \theta_2$ and T = 180° for all of the complexes due to the crystal symmetry. Further, the M-X···X angle θ is nearly identical in all cases, leaving the only significant difference the expected longer X···X separation for the bromide complexes (average ~3.74 Å) compared to the chloride complexes (average ~ 3.59 Å).

Finally, complexes **5-8** exhibit Type II halogen bonds between the chloro-substituents on the aniline ligands as seen in Figure 4b [the d, θ_1, θ_2 values for **5-8** are: **5** - d = 3.523 Å, θ_1 = 144.6° and θ_2 = 89.5°; **6** - 3.525 Å, 144.43°, 89.62°; **7** - 3.633 Å, 139.23°, 87.812°; **8** - 3.631 Å, 139.23°, 87.73°). The d-values are slightly longer for the bromide complexes, as expected, and interestingly, both the θ_1, θ_2 angles are smaller in the bromide complexes.

Fitting of the magnetic data for compounds **1**, **3**, **5**, and **7** shows small differences in the *g*-factor (2.3-2.4) within the range expected for tetrahedral Co(II) complexes.[55] The consistency of g-factor and very nearly tetrahedral geometry suggest that single-ion anisotropy effect are negligible in the samples over the temperature range in question and thus were not included in the final simulations. The primary question comes in regard to the potential superexchange pathway(s) in the systems and the distinctly different behavior observed between the cobalt chloride and cobalt bromide complexes. The magnetic properties appear to be independent of the substituent on the aniline ligand and thus we focus our

attention on the hydrogen bonding and on the two-halide pathway and halide…metal contacts. The intermolecular halide…Co contacts are shorter for the cobalt chloride compounds (**1**, **5**) by ~ 0.04Å, which is not commensurate with the decrease in radius (~0.1Å) between Br and Cl, suggesting that this superexchange pathway may be stronger in the bromide complexes and potentially dominate, in agreement with the good fit provided by the 1D-chain model for compounds **3** and **7**. Use of an additional parameter (α) with the rectangular model does not significantly improve the fit and the resulting values for C and J are nearly identical. This is not true for the cobalt chloride complexes **1** and **5** however. As seen in the temperature dependence of χ(T) and χT(T), there are additional factors and discontinuities which occur at two different temperatures (as shown in the χ vs. T and χT vs. T plots), suggesting the presence of a more complex magnetic lattice and superexchange network. With respect to the two-halide pathway parameters (vide supra), the only significant difference is the shorter Cl…Cl distances (~ 0.2 Å) observed, which would be expected to produce a stronger magnetic exchange given the equivalence of the other parameters. This may be sufficient for this second pathway to compete with the short halide…Co pathway and provided for a complex, 2D-magnetic lattice.

Conclusions

A family of ML_2X_2 complexes (M = Co, Zn; X = Cl, Br; L = 4-methylaniline, 4-chloroaniline) has been prepared and characterized via single-crystal X-ray analysis and temperature dependent magnetic susceptibility. All eight complexes show the same local coordination geometries about the metal ion with small differences in the structural parameters due to the differences in halide ion. The compounds pack in two different fashions as a result of halogen bonding occurring through the chlorine substituents of the 4-chloroaniline ligands. Magnetic susceptibility measurements on the cobalt complexes all show a maximum in the susceptibility at low temperature (~ 4 K) indicative of antiferromagnetic interactions, but the temperature dependence suggests different magnetic lattices are in force between the bromide and chloride complexes, most likely as a result of the expected changes in orbital overlap. Additional data will be required to provide a more quantitative analysis of the differences and work is in progress to prepare additional members of this family of compounds.

Acknowledgements

Financial support from the Carlson School of Chemistry and Biochemistry, Clark University and the Department of Chemistry, Brandeis University, is gratefully recognized. The assistance of Mr. Arjuna Shenoy in the preparation of compound **2** is appreciated. We would like to thank Mr. Dave Liles and Dr. Frikkie Malan for assistance with X-ray data collections. F. X. would like to acknowledge the funding from the European Union's Horizon 2020 research and innovation program under the Marie Skodowska-

Curie grant agreement No 701647. The simulations were performed on UBELIX (http://www.id.unibe.ch/hpc), the HPC cluster at the University of Bern.

Supplementary Information

Figures showing the molecular units of **2-4** and **6-8** (Figures S1-S6), figures showing the χ vs. H data for compounds **5** and **7** (Figures S7-S8) and a description of the procedure used for simulation of the susceptibility data (SI-1) are presented.

CCDC 1854458(**5**), 1854459(**1**), 1854460(**2**), 1854461(**7**), 1854462(**6**), 1854463(**4**), 1854464(**3**), 1854465(**8**) contains the supplementary crystallographic data for **1-8**. These data can be obtained free of charge via https://www.ccdc.cam.ac.uk/structures/, or from the Cambridge Crystallographic Data Centre, 12 Union Road, Cambridge CB2 1EZ, UK; fax: (+44) 1223-336-033; or e-mail: deposit@ccdc.cam.ac.uk.

References:

1. J. Ferrando-Soria, J. Vallejo, M. Castellano, J. Martinez-Lillo, E. Pardo, J. Cano, I. Castro, F. Lloret, R. Ruiz-Garcia and M. Julve, *Coord. Chem. Rev.* 2017, **339,** 17.
2. X. Zhang, L. W. Chung and Y. D. Wu, *Acc. Chem. Res.* 2016, **49,** 1302.
3. J. Ferrando-Soria, M. Castellano, E. Pardo, J. Cano, F. Lloret, R. Ruiz-Garcia, J. Ferrando-Soria, F. Fortea-Perez, S. E. Stiriba and M. Julve, *Acc. Chem. Res.* 2015, **48,** 510.
4. A.V. Funes and P. Alboreslo, *Eur. J. Inorg. Chem.* 2018, **2018**, 2067.
5. M. Murrie, *Polyhedron*, 2018, **150**, 1.
6. G. Cosquer, Y. Shen, M. Almeida, and M. Yamashita, *Dalton Trans.* 2018, **47**, 7616.
7. J. Lu, M. Guo and J. Tang, *Chem.-Asian J.* 2017, **12**, 2772.
8. D.-X. Bao, S. Xiang, J. Wang, Y.-C. Li, X.-Q. Zhao, *J. Coord. Chem.* 2016, **69**, 3131.
9. Y. Journaux, J. Ferrando-Soria, E. Pardo, R. Ruiz-Garcia, M. Julve, F. Lloret, J. Cano, Y. Li, L. Lisnard, P. Yu, Pei; H. Stumpf and C.L.M. Pereira, *Eur. J. Inorg. Chem.* 2018, **2018**, 228.
10. K. Liu, X. Zhang, X. Meng, W. Shi, P. Cheng and A.K. Powell, *Chem. Soc. Rev.* 2016, **45**, 2423.
11. C. Coulon, V. Pianet, M. Urdampilleta and R. Clerac, *Struct. and Bond.* 2015, **164,** 143.
12. F. Pointillart, O. Cador, B. Le Guennic and L. Ouahab *Coord. Chem. Rev.* 2017, **346**, 150.
13. M. Feng and M.-L. Tong, *Chem. – Eur. J.* 2018, **24**, 7574.
14. J.M. Frost, K.L. Harriman and M. Murugesu, *Chem. Sci.* 2016, **7**, 2470.
15. P. Cen, X. Ma, X. Liu, Y.-Q. Zhang, G. Xie and S. Chen, *J. Coord. Chem.* 2018, **71**, 2209.
16. M. Ashafaq, M. Raizada, M. Khalid, M. Shahid, M. Ahmad Z.A. Siddiqi, *J. Coord. Chem.* 2018, **71**, 2118.
17. Q. Gao, Z. Lin, M. Duan, D. Li, X. Li, Y. Wu, D. Hu, *J. Coord. Chem.* 2018, **71**, 2109.
18. C.F.N. Nguemdzi, F. Capet, J. Ngoune, G. Bebga, M. Foulon, J. Nenwa, *J. Coord. Chem.* 2018, **71**, 1484.
19. M. Zirak, E. Jamali Garegeshlagi, *J. Coord. Chem.* 2018, **71**, 1168.
20. L. Martinez, L. Arizaga, D. Armentano, F. Lloret, R. Gonzalez, C. Kremer, R. Chiozzone, *J. Coord. Chem.* 2018, **71**, 748.

21. J. Lengyel, S.A. Stoian, N. Dalal, M. Shatruk, *Polyhedron* 2018, **151**, 446.
22. O. Drath, R.W. Gable, B. Moubaraki, K.S. Murray, C. Boskovic, *Polyhedron* 2018, **151**, 323.
23. B.W. Stein, C.R. Tichnell, J. Chen, D.A. Shultz, M.L. Kirk, *J. Am. Chem. Soc.* 2018, **140**, 2221.
24. Y. Homma, T. Ishida, *Chem. Mater.* 2018, **30**, 1835.
25. R.F. Higgins, B.N. Livesay, T.J. Ozumerzifon, J.P. Joyce, A.K. Rappe, M.P. Shores, *Polyhedron* 2018, **143**, 193.
26. J. Martinez-Lillo, D. Armentano, F.R. Fortea-Perez, S.-E. Stiriba, G. De Munno, F. Lloret, M. Julve, J. Faus, *Inorg. Chem.* 2015, **54**, 4594.
27. M. Idesicova, R. Boca, *Inorg. Chim. Acta* 2013, **408**, 162.
28. J. Anagnostis, J. Cipi, C.P. Landee, G.W. Tremelling, M.M. Turnbull, B. Twamley, J.L. Wikaira, *J. Coord. Chem.* 2017, **70**, 3892.
29. S.N. Herringer, C.P. Landee, M.M. Turnbull, J. Ribas-Arino, J.J. Novoa, M. Polson, J.L. Wikaira, *Inorg. Chem.* 2017, **56**, 5441.
30. C.A. Krasinski, B.L. Solomon, F.F. Awwadi, C.P. Landee, M.M. Turnbull, J.L. Wikaira, *J. Coord. Chem.* 2017, **70**, 914.
31. R.T. Butcher, M.M. Turnbull, C.P. Landee, A. Shapiro, F. Xiao, D. Garrett, W. Robinson, B. Twamley, *Inorg. Chem.* 2010, **49**, 427.
32. C.P. Landee, J.C. Monroe, R. Kotarba, M. Polson, J.L. Wikaira, M. M. Turnbull, *J. Coord. Chem.* 2018, **71**, 3342.
33. A.D. Richardson, T.J. Zirkman, M.T. Kebede, C.P. Landee, M. Rademeyer, M.M. Turnbull, *Polyhedron* 2018, **147**, 106.
34. J. Bonire, N. Jalil, G. A. Ayoko and A. Omachi, *Appl. Organomet. Chem*. 1996, **10,** 366.
35. N. Kumari, V. K. Yadav, S. Zalis and L. Mishra, *Ind. J. Chem*. 2012, **51A,** 554.
36. R.A.Burrow, M.Horner, L.S.Lang, A.Neves, I.Vencato *Z.Kristallogr.-New Cryst.Struct.* 1997, **212**, 41.
37. S.Low, J.Becker, C.Wurtele, A.Miska, C.Kleeberg, U.Behrens, O.Walter, S.Schindler *Chem.-Eur.J.* 2013, **19**, 5342.
38. a) Ejaz, O. Sahin, I.U.Khan *Acta Crystallogr.,Sect.E* 2009, **65**, m1457. b) M. Rademeyer, *Acta Crystallogr.,Sect.E:* **60**, m871, 2004. c) I.U.Khan, Ejaz, O.Sahin, O. Buyukgungor *Acta Crystallogr.,Sect.E* 2010, **66**, m492.
39. a) Y.-B. Chen, Z.-J. Li, Y.-Y. Qin, Y. Kang, L. Wu, Y.-G. Yao, *Jiegou Huaxue(Chin.) (Chin.J.Struct.Chem.)* 2002, **21**, 530. b) V.A. Kozlov, D.V. Aleksanyan, Yu.V. Nelyubina, K.A.. Lyssenko, A.A. Vasil'ev, P.V. Petrovskii, I.L. Odinets *Organometallics* 2010, **29**, 2054.
40. a) C.E. Costin-Hogan, C.-L. Chen, E. Hughes, A. Pickett, R. Valencia, N.P. Rath, A.M. Beatty *CrystEngComm* 2008, **10**, 1910. b) A. Harmouzi, N. Daro, P. Guionneau, A. Belaaraj, El M. Khechoubi *J.Cryst.Growth* 2017, **472**, 64. c) F.D. Rochon, C. Bonnier *Inorg. Chim. Acta* 2007, **360**, 461.
41. a) R.N. Akatova, T.N. Tarkhova, N.V. Belov *Kristallografiya(Russ.)(Crystallogr.Rep.)* 1982, **27**, 1187. b) T.I. Malinovskii *Kristallografiya(Russ.)(Crystallogr.Rep.)* 1957, **2**, 734.
42. J. Govindaraj, S. Thirumurugan, D.S. Reddy, K. Anbalagan, A. Subbiah Pandi *Acta Crystallogr.,Sect.E* 2105, **71**, m21.
43. a) V.M. Padmanabhan, R.P. Patel, T.N. Ranganathan *Acta Crystallogr.,Sect.C:* 1985, **41**, 1305. b) A. Grirrane, H. Garcia, A. Corma, E. Alvarez *Chem.-Eur. J.* 2012, **18**, 14934. c) A. Subashini, K. Ramamurthi, H. Stoeckli-Evans *Acta Crystallogr.,Sect.E* 2012, **68**, m1152.
44. T. Matsumoto, Y. Miyazaki, A.S. Albrecht, C.P. Landee, M.M. Turnbull, M. Sorai, *J. Phys. Chem. B*., 2000, **104**, 9993.
45 P. O. Dunstan, *Thermochimica Acta*. 2006, **450**, 5.
46 R. L. Carlin. *Magnetochemistry*; Springer-Verlag: Berlin, 1986.
47. Bruker AXS Inc., Madison, WI, USA, (2012)
48 G.M. Sheldrick *Acta Cryst. A* 2008, **64**, 112.
49. G.M. Sheldrick *Acta Cryst.* 2015, **C71**, 3.
50. L. Takacs *Chem. Soc. Rev.* 2013, **42**, 7649.

51. Turnbull, M.M.; Landee, C.P.; Wells, B.M. *Coord. Chem. Rev*. 2005, **249**, 2567-2576.
52. Fisher, M. E. *Am. J. Phys.* 1964, **32**, 343–346.
53. B. Bauer, L.D. Carr, H.G. Evertz, A. Feiguin, J. Freire, S. Fuchs, L. Gamper, J. Gukelberger, E. Gull, S. Guertler, A. Hehn, R. Igarashi, S.V. Isakov, D. Koop, P.N. Ma, P. Mates, H. Matsuo, O. Parcollet, G. Pawłowski, J.D. Picon, L. Pollet, E. Santos, V.W. Scarola, U. Schollwöck, C. Silva, B. Surer, S. Todo, S. Trebst, M. Troyer, M.L. Wall, P. Werner and S. Wessel (ALPS collaboration) *J. Stat. Mech.* 2011, P05001.
54. G.P. Guedes, F.F. Farias, M.A. Novak, F.L.de A.Machado, M.G.F. Vaz *Inorg.Chim.Acta* 2011, **378**, 134.
55. a) O.B. Ona, D.R. Alcoba, G.E. Massaccesi, A. Torre, L. Lain, J.I. Melo, J.M. Oliva-Enrich, J.E. Peralta, *Inorg. Chem.* 2019, **58**, 2550. b) T.F.C. Cruz, C.A. Figueira, J.C. Waerenborgh, L.C. Pereira, Y. Li, R. Lescouezec, P.T. Gomes, *Polyhedron* 2018, **152**, 179. c) A. Switlicka, B. Machura, R. Kruszynski, J. Cano, L.M. Toma, F. Lloret, M. Julve, *Dalton Trans.* 2018, **47**, 5831.